

Iron Emission Lines on the Galactic Ridge Observed with Suzaku

Shigeo YAMAUCHI,¹ Ken EBISAWA,² Yasuo TANAKA,³ Katsuji KOYAMA,⁴ Hironori MATSUMOTO,⁴
Noriko Y. YAMASAKI,² Hiromitsu TAKAHASHI,⁵ and Yuichiro EZOE,⁶

¹*Faculty of Humanities and Social Sciences, Iwate University, 3-18-34 Ueda, Morioka, Iwate 020-8550
yamauchi@iwate-u.ac.jp*

²*Institute of Space and Astronautical Science/JAXA, 3-1-1 Yoshinodai, Sagami-hara, Kanagawa 229-8510*

³*Max-Planck-Institut für extraterrestrische Physik, D-85748 Garching, Germany*

⁴*Department of Physics, Graduate School of Science, Kyoto University, Sakyo-ku, Kyoto, 606-8502*

⁵*Department of Physical Science, School of Science, Hiroshima University,*

1-3-1 Kagamiyama, Higashi-Hiroshima, Hiroshima, 739-8526

⁶*Department of Physics, Tokyo Metropolitan University, 1-1 Minami-Osawa, Hachioji, Tokyo 192-0397*

(Received ; accepted)

Abstract

In order to elucidate origin of the Galactic Ridge X-ray Emission, we analyzed Suzaku data taken at various regions along the Galactic plane and studied their Fe-K emission line features. Suzaku resolved the Fe line complex into three narrow lines at ~ 6.4 keV, ~ 6.7 keV and ~ 6.97 keV, which are K-lines from neutral (or low-ionized), He-like, and H-like iron ions, respectively. The 6.7 keV line is clearly seen in all the observed regions and its longitudinal distribution is consistent with that determined from previous observations. The 6.4 keV emission line was also found in various Galactic plane regions ($b \sim 0^\circ$). Differences in flux ratios of the 6.4 keV/6.7 keV and 6.97 keV/6.7 keV lines between the Galactic plane and the Galactic center regions are studied and its implication is discussed.

Key words: Galaxy: disk — X-rays: diffuse background — X-rays: ISM — X-rays: stars — X-rays: spectra

1. Introduction

The Galactic Ridge X-ray Emission (GRXE) is unresolved X-ray emission along the Galactic plane (e.g., Worrall et al. 1982; Warwick et al. 1985; Koyama et al. 1986; Yamauchi et al. 1996; Kaneda et al. 1997; Sugizaki et al. 2001; Ebisawa et al. 2001; Tanaka 2002; Revnivtsev et al. 2006). Previous observations with several X-ray satellites have revealed spectral characteristics of the GRXE. The GRXE spectrum exhibits emission lines from highly ionized Si, S and Fe, and the 3–10 keV continuum spectrum is represented by a thin thermal emission model with a temperature of ~ 5 –10 keV (Koyama et al. 1986; Kaneda et al. 1997; Sugizaki et al. 2001). Additionally, a significant excess from the thermal emission is found above 10 keV (Yamasaki et al. 1997; Valinia & Marshall 1998).

Spatial distribution of the GRXE is very similar to the Galactic structure (Warwick et al. 1985; Yamauchi & Koyama 1993), and traces near infrared emission (Revnivtsev et al. 2006). Fluctuation analysis using the ASCA data has given a constraint on the X-ray point sources contributing to the GRXE: the number density is larger than $110 (3' \times 3')^{-1}$ and the averaged flux is smaller than 10^{-14} erg s $^{-1}$ cm $^{-2}$ (Sugizaki et al. 1999). If the unresolved faint X-ray sources are located in the 4 kpc arm, number of the sources in the Galaxy (N) and their luminosity (L_X) should be $N > 1.4 \times 10^7$ and $L_X < 1.9 \times 10^{31}$ erg s $^{-1}$ (2–10 keV), respectively (Sugizaki et al. 1999). Meanwhile, a deep observation with Chandra resolved

only ~ 10 % or ~ 19 % of the GRXE flux into discrete sources with an X-ray flux (F_X) of $F_X > 3 \times 10^{-15}$ erg s $^{-1}$ cm $^{-2}$ in the 2–10 keV band (Ebisawa et al. 2001, 2005) or $F_X > 1.2 \times 10^{-15}$ erg s $^{-1}$ cm $^{-2}$ in the 1–7 keV band (Revnivtsev & Sazonov 2007), respectively.

While our observational knowledge on the GRXE has significantly increased since its discovery, origin of the GRXE remains unsolved. The most important issue is whether the GRXE is truly diffuse emission or composition of numerous faint X-ray sources. However, in either way, problems still remain: If the diffuse origin is right, the hot plasma gas having a huge thermal energy ($\sim 10^{56}$ erg, a filling factor = 1) is hard to be confined by the Galactic gravity. What is the mechanism to produce and maintain such a hot plasma gas in the Galaxy? On the other hand, if the point source model is correct, what kind of sources are they? The sources are required to have a thin thermal emission ($kT=5$ –10 keV) with strong Fe-K emission lines, similar to the GRXE.

Systematic study of the GRXE spectra is important to solve origin of the GRXE. Suzaku has better spectral resolution, wider energy band, and lower/more stable intrinsic background than previous X-ray satellites (Mitsuda et al. 2007). Therefore, Suzaku is the best instrument to study diffuse sources with low surface brightness such as the GRXE. In fact, the 100 ks observation in the Scutum region of (l, b)=(28.46, -0.20) with Suzaku for the first time revealed that the Fe line complex consists of three narrow emission lines, which are K-lines from neutral or

Table 1. Observation logs.

Position ID	Sequence No.	(l, b)	Observation time (UT)		Exposure (ksec)
			Start	End	
Galactic Ridge X-Ray Emission (GRXE)					
R1	100028020	$(332^{\circ}00, -0^{\circ}15)$	2005-09-18 22:36 – 2005-09-19 11:58		18
R2	100028010	$(332^{\circ}40, -0^{\circ}15)$	2005-09-19 11:58 – 2005-09-20 19:38		40
R3	100028030	$(332^{\circ}70, -0^{\circ}15)$	2005-09-20 19:38 – 2005-09-21 07:29		21
R4	100026030	$(345^{\circ}80, -0^{\circ}54)$	2005-09-28 07:06 – 2005-09-29 04:25		37
R5	100026020	$(347^{\circ}63, 0^{\circ}71)$	2005-09-25 19:02 – 2005-09-26 15:42		29
R6	500008010	$(8^{\circ}04, -0^{\circ}05)$	2006-04-07 11:48 – 2006-04-08 10:54		40
R7	500007010	$(8^{\circ}44, -0^{\circ}05)$	2006-04-06 14:13 – 2006-04-07 11:48		37
R8	500009010	$(28^{\circ}46, -0^{\circ}20)$	2005-10-28 02:24 – 2005-10-30 21:30		83
Galactic Center Diffuse X-Ray Emission (GCDX)					
GC1	500019010	$(358^{\circ}91, -0^{\circ}04)$	2006-02-23 10:50 – 2006-02-23 20:02		13
GC2a	100027020	$(359^{\circ}75, -0^{\circ}05)$	2005-09-24 14:16 – 2005-09-25 17:27		37
GC2b	100037010	$(359^{\circ}75, -0^{\circ}05)$	2005-09-29 04:25 – 2005-09-30 04:29		43
GC3a	100027010	$(0^{\circ}06, -0^{\circ}07)$	2005-09-23 07:07 – 2005-09-24 11:05		44
GC3b	100037040	$(0^{\circ}06, -0^{\circ}07)$	2005-09-30 07:41 – 2005-10-01 06:21		42
GC4	100037070	$(1^{\circ}00, -0^{\circ}10)$	2005-10-12 07:05 – 2005-10-12 11:05		9

low ionized (6.4 keV), He-like (6.68 keV), and H-like (6.97 keV) irons (Ebisawa et al. 2008). In particular, existence of the 6.4 keV line on the Galactic plane raises a new question on its origin, because the 6.4 keV line is not expected from a thin thermal plasma. It has not yet been known whether the spectral properties of the GRXE, in particular the Fe-line features, in all of the Galactic plane regions are the same or not. In order to examine spectral and spatial variations of the GRXE, we are going to analyze the GRXE spectra obtained with Suzaku in various regions on the Galactic plane and in the Galactic center (GC) region and compare their iron line features.

2. Observations and Data Reduction

Suzaku observations of the Galactic plane were carried out with 4 X-ray CCD camera systems (XIS, Koyama et al. 2007a) placed at the focal plane of the thin-foil X-ray Telescopes (XRT, Serlemitsos et al. 2007), and with the co-aligned non-imaging Hard X-ray Detector (HXD, Takahashi et al. 2007; Kokubun et al. 2007). In order to compare the spectral features of the thermal component, especially iron line features of the GRXE, we concentrate on the XIS data analysis in this paper.

XIS sensor-1 (XIS1) has a back-illuminated CCD (BI), while the other three XIS sensors (XIS0, 2, and 3) have front-illuminated CCDs (FI). The XIS was operated in the normal clocking mode. The field of view (FOV) of the XIS is $17.8' \times 17.8'$. The non-X-ray background level of the FI detectors is lower than that of the BI detector, and the sensitivity of the FI detector in the Fe band is better than that of the BI detectors (Koyama et al. 2007a). Therefore, in order to achieve the highest signal-to-noise ratio in the Fe band, we used only the FI detectors.

We selected the Galactic plane fields at $|b| < 1^{\circ}$ which are devoid of significant point sources (position ID: R1–8). Galactic locations and observation dates of the data used for the present analysis are listed in table 1. We note that the data of R8 are the same as those used in Ebisawa et al. (2008). We also analyzed the data of R8 in the same process. In order to compare the iron line features of the GRXE with those of the Galactic center diffuse X-ray emission (GCDX) (Koyama et al. 1989; Yamauchi et al. 1990), we also selected data observed near the GC (position ID: GC1–4, see table 1).

Data reduction and analysis were made using the HEADAS software version 6.2 and version 1.2 of the processed data. We excluded the data obtained at the South Atlantic Anomaly, during Earth occultation, and at low elevation angles from the Earth rim of $< 5^{\circ}$ (night Earth) or $< 20^{\circ}$ (day Earth). We also removed the XIS hot and/or flickering pixels. The resultant exposure time is also listed in table 1.

3. Analysis and Results

In order to construct the GRXE spectra, we extracted X-ray photons from the entire region of the XIS FOV, excluding the point-like sources in the FOV and the calibration sources located at corners of the XIS sensors. We also excluded the Sgr A complex (Sgr A* and Sgr A East) from the GC2 and GC3 data. To maximize the photon statistics, data obtained with XIS0, 2, and 3 were combined. Furthermore, data obtained at the same pointing positions (GC2a&GC2b and GC3a&GC3b) were also combined. The response files, Redistribution Matrix Files (RMFs) and Ancillary Response Files (ARFs), were made for each pointing using `xisrmfgen` and `xissimarfgen`, re-

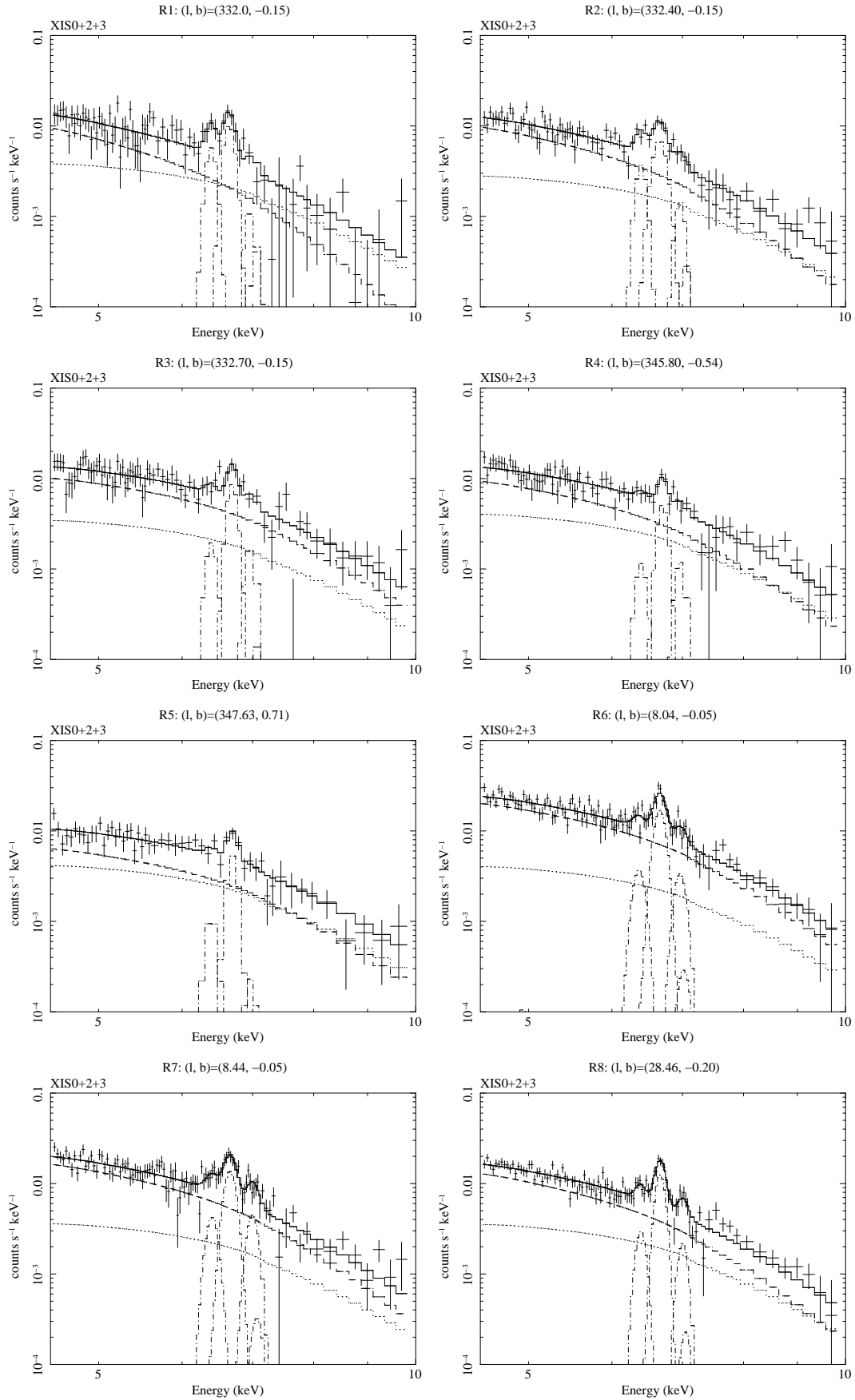


Fig. 1. The background-subtracted the GRXE spectra observed in the various regions (see table 1). The data obtained with XIS0, 2, and 3 were combined. The dashed, dotted, and dash-dotted lines show contributions of the bremsstrahlung, power-law (CXB), and emission line models, respectively.

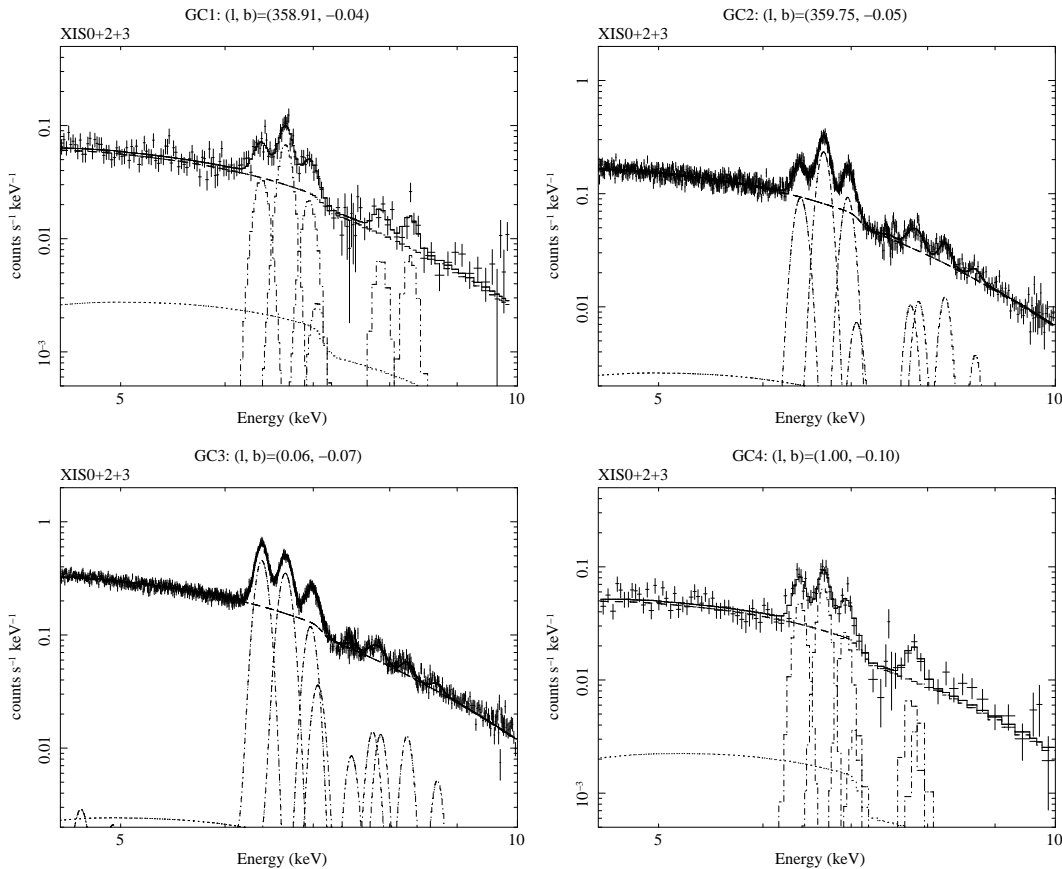


Fig. 2. The same as figure 1, but the GCDX spectra (see table 1).

spectively, in HEADAS software version 6.2. In making ARF for the diffuse GRXE, flat photon distribution with a radius of $20'$ was assumed. Non-X-ray background was calculated using the background database provided by the XIS team (Tawa et al. 2008).

In the observed Suzaku spectra, we found many emission lines from highly ionized ions, such as Mg, Si, S, and Fe, while in the present paper we focus on the Fe line feature. Figure 1 shows the observed FI spectra in the 4.5–10.0 keV energy band after subtraction of the non-X-ray background. We can clearly see three emission lines in the 6–7 keV range, which are K-lines from neutral (or low ionized), He-like, and H-like iron. In order to measure the emission line parameters, we fitted the spectra with the following model;

For the GRXE

Absorption \times (thermal bremsstrahlung+Gaussian lines)

For the Cosmic X-ray Background (CXB)

Absorption \times power-law (Γ and N_{PL} ; fixed)

The cross sections of photoelectric absorption are taken from Balucinska-Church and McCammon (1992). The normalization (N_{PL}) and photon index (Γ) of the power-law model was fixed to be 10 photons $\text{s}^{-1} \text{cm}^{-2} \text{sr}^{-1} \text{keV}^{-1}$ at 1 keV (e.g., Gendreau et al. 1995; Revnivtsev et al. 2005) and 1.4 (Marshall et al. 1989), respectively. Absorption column densities for the GRXE and the CXB

are fixed at $N_{\text{H}}=3\times 10^{22} \text{cm}^{-2}$ and $6\times 10^{22} \text{cm}^{-2}$, respectively (Ebisawa et al. 2001). Three emission lines of Fe I $K\alpha$ (6.4 keV), Fe XXV $K\alpha$ (6.7 keV), and Fe XXVI $K\alpha$ (6.97 keV) are considered in the model fitting. In addition, $K\beta$ line from Fe I is considered, whose center energy and intensity are assumed to be $1.103 \times$ that of Fe I $K\alpha$ and $0.1 \times$ that of Fe I $K\alpha$, since they are not constrained from the data. The best-fit model is also plotted in figure 1 and the best-fit parameters of the Fe-lines are listed in table 2. The center energies of three emission lines have been constrained as 6.36–6.41, 6.65–6.71, and 6.97–7.01 keV. Thus, Suzaku clearly resolved the Fe line complex into K-lines from Fe I, Fe XXV, and Fe XXVI, for all the Galactic plane regions. No significant broadening in the Fe line width was found.

In order to obtain the iron line fluxes from the GCDX, we applied the same process to the GC data. We constructed the GCDX spectra excluding the Sgr A complex and point-like sources in the FOV. The absorption column for the GCDX was fixed to $N_{\text{H}}=6\times 10^{22} \text{cm}^{-2}$ (Sakano et al. 2002) and that for CXB was set to be twice of the value for the GCDX; $N_{\text{H}}=12\times 10^{22} \text{cm}^{-2}$. As noted in Koyama et al. (2007c), a clear absorption edge of neutral or lower ionized iron was found at 7.1 keV in the spectra, so we set the Fe abundance in the absorption column free. In addition, emission lines of Ni I $K\alpha$ (7.49 keV), Ni XXVII $K\alpha$ (7.77 keV), Fe XXV $K\beta$ (7.88 keV), Fe XXVI $K\beta$ (8.25

Table 2. Parameters obtained from a spectral analysis for the spectra in the 4.5–10.0 keV.*

Parameter	Value							
	R1	R2	R3	R4	R5	R6	R7	R8
kT^\dagger	$2.6^{+1.8}_{-0.9}$	$3.9^{+1.8}_{-1.1}$	$10.8^{+36.0}_{-5.3}$	$5.4^{+5.2}_{-2.1}$	$8.6^{+35.6}_{-4.4}$	$6.0^{+2.0}_{-1.4}$	$5.1^{+2.1}_{-1.3}$	$4.1^{+1.2}_{-0.8}$
$E_{6.4\text{keV}}^\ddagger$	6.40 (fixed)	6.40 (fixed)	6.40 (fixed)	6.40 (fixed)	6.40 (fixed)	6.37±0.06	$6.41^{+0.07}_{-0.06}$	$6.39^{+0.05}_{-0.03}$
$\sigma_{6.4\text{keV}}^\S$	0 (fixed)	0 (fixed)	0 (fixed)	0 (fixed)	0 (fixed)	<133	0 (fixed)	<84
$I_{6.4\text{keV}}^\parallel$	2.5 ± 1.3	$2.2^{+1.1}_{-1.2}$	<2.2	<1.3	<1.4	1.8 ± 1.0	2.3 ± 1.2	$1.4^{+0.7}_{-0.6}$
$EW_{6.4\text{keV}}^\#$	390 ± 200	190^{+90}_{-100}	<160	<150	<190	90 ± 50	140^{+70}_{-80}	110^{+60}_{-50}
$E_{6.7\text{keV}}^\ddagger$	$6.65^{+0.04}_{-0.03}$	$6.67^{+0.03}_{-0.04}$	6.70 ± 0.04	$6.71^{+0.03}_{-0.04}$	6.70 ± 0.04	$6.666^{+0.014}_{-0.013}$	6.668 ± 0.017	$6.674^{+0.009}_{-0.012}$
$\sigma_{6.7\text{keV}}^\S$	<103	65^{+54}_{-57}	0 (fixed)	<77	<78	<38	<65	<36
$I_{6.7\text{keV}}^\parallel$	$5.5^{+1.9}_{-1.6}$	$6.2^{+1.7}_{-1.6}$	$4.8^{+1.4}_{-1.5}$	2.4 ± 0.9	$2.5^{+1.0}_{-0.9}$	9.1 ± 1.2	$8.7^{+1.7}_{-1.5}$	6.6 ± 0.8
$EW_{6.7\text{keV}}^\#$	980^{+330}_{-280}	600^{+170}_{-150}	380 ± 120	300 ± 110	400^{+160}_{-150}	510 ± 70	570 ± 100	590 ± 70
$E_{6.97\text{keV}}^\ddagger$	6.97 (fixed)	6.97 (fixed)	6.97 (fixed)	6.97 (fixed)	6.97 (fixed)	6.97±0.06	$7.00^{+0.07}_{-0.05}$	$7.01^{+0.03}_{-0.04}$
$\sigma_{6.97\text{keV}}^\S$	0 (fixed)	0 (fixed)	0 (fixed)	0 (fixed)	0 (fixed)	<109	0 (fixed)	<45
$I_{6.97\text{keV}}^\parallel$	<1.8	1.1 ± 1.0	<2.4	<1.5	<1.0	$2.1^{+1.0}_{-1.1}$	$3.1^{+1.3}_{-1.2}$	1.3 ± 0.7
$EW_{6.97\text{keV}}^\#$	<390	120 ± 110	<210	<210	<170	130 ± 70	230 ± 90	140 ± 70
χ^2_{ν} (d.o.f.)	0.95 (69)	0.97 (71)	0.96 (70)	0.90 (70)	0.74 (47)	1.20 (95)	1.14 (97)	1.19 (95)
	GC1	GC2	GC3	GC4				
kT^\dagger	$11.7^{+7.2}_{-3.3}$	$13.0^{+1.5}_{-1.0}$	10.8 ± 0.6	$18.0^{+24.2}_{-7.8}$				
$E_{6.4\text{keV}}^\ddagger$	$6.397^{+0.019}_{-0.020}$	$6.411^{+0.006}_{-0.005}$	6.402 ± 0.002	$6.404^{+0.017}_{-0.013}$				
$\sigma_{6.4\text{keV}}^\S$	<68	<38	<10	<46				
$I_{6.4\text{keV}}^\parallel$	17 ± 4	45 ± 3	229^{+4}_{-5}	24 ± 5				
$EW_{6.4\text{keV}}^\#$	200 ± 50	180 ± 20	440 ± 10	270 ± 60				
$E_{6.7\text{keV}}^\ddagger$	6.673 ± 0.010	$6.675^{+0.003}_{-0.002}$	$6.671^{+0.003}_{-0.002}$	6.676 ± 0.012				
$\sigma_{6.7\text{keV}}^\S$	<28	<22	24^{+5}_{-6}	<46				
$I_{6.7\text{keV}}^\parallel$	36 ± 4	119^{+4}_{-3}	202^{+5}_{-4}	36 ± 6				
$EW_{6.7\text{keV}}^\#$	450^{+60}_{-50}	510 ± 20	420^{+20}_{-10}	420^{+80}_{-70}				
$E_{6.97\text{keV}}^\ddagger$	6.95 ± 0.03	6.962 ± 0.004	$6.970^{+0.004}_{-0.005}$	$6.93^{+0.03}_{-0.02}$				
$\sigma_{6.97\text{keV}}^\S$	<53	<14	<16	<49				
$I_{6.97\text{keV}}^\parallel$	13 ± 4	52 ± 3	72^{+4}_{-3}	16 ± 5				
$EW_{6.97\text{keV}}^\#$	180 ± 60	240^{+20}_{-10}	160^{+20}_{-10}	200 ± 60				
χ^2_{ν} (d.o.f.)	1.03 (146)	1.03 (853)	1.07 (1010)	1.11 (85)				

* Errors show single-parameter 90% confidence levels.

† Temperature of the thermal bremsstrahlung model in the unit of keV.

‡ Energy of the emission line in the unit of keV.

§ Width of the emission line in the unit of eV.

|| Intensity of the emission line in the unit of $\times 10^{-8}$ counts s^{-1} cm^{-2} arcmin^{-2} .

Equivalent width in the unit of eV.

keV), Fe XXV $K\gamma$ (8.29 keV), and Fe XXVI $K\gamma$ (8.70 keV) have been found in the GCDX spectra (Koyama et al. 2007c). Therefore, we added these emission lines to the model, if they are found in the spectra. In this analysis, the line center energy and the intrinsic line width were fixed to the predicted values and null, respectively. The best-fit model is plotted in figure 2 and the best-fit parameters of Fe-lines are listed in table 2.

Figure 3 shows the 6.4 keV, 6.7 keV, and 6.97 keV emission line fluxes as a function of the Galactic longitude, which demonstrates a significant enhancement of the emission line fluxes at the GC. The intensities of the Fe-lines in the R4 and R5 regions, which are >0.5 apart from the Galactic plane, are systematically lower than those in the other Galactic plane regions (R1–3, 6–8), because

the GRXE intensity decreases with the height from the Galactic plane (Yamauchi & Koyama 1993; Kaneda et al. 1997). Taking account of the galactic latitude-dependence of the GRXE intensity, the 6.7 keV line distribution is consistent with those obtained in previous observations (Koyama et al. 1989; Yamauchi & Koyama 1993; Sugizaki et al. 2001). The 6.4 keV line is also found in the various Galactic plane regions ($b \sim 0^\circ$) and particularly conspicuous close to the GC.

Figure 4 shows the flux ratios of the 6.4 keV/6.7 keV and 6.97 keV/6.7 keV lines. The 6.4 keV/6.7 keV ratios for the GCDX are significantly larger than those for the GRXE and the 6.97 keV/6.7 keV ratios also show similar tendency.

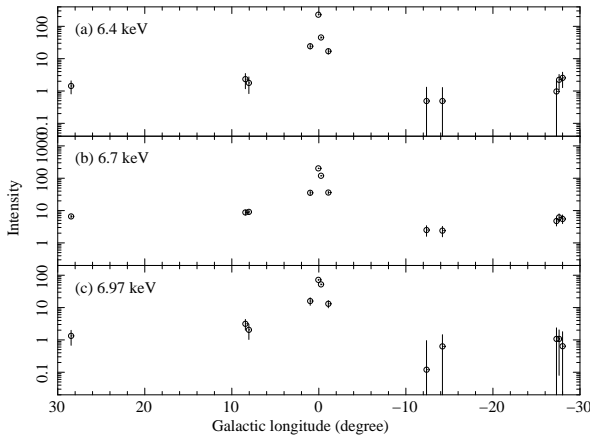


Fig. 3. (a) 6.4 keV, (b) 6.7 keV, and (c) 6.97 keV line fluxes as a function of the Galactic longitude. The unit of the line flux is $\times 10^{-8}$ count s^{-1} cm^{-2} $arcmin^{-2}$. The error shows the 90 % confidence level.

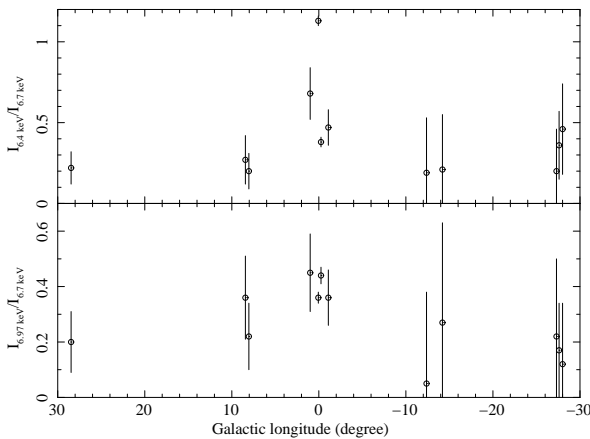


Fig. 4. The flux ratios of 6.4 keV/6.7 keV (upper) and 6.97 keV/6.7 keV (lower) lines as a function of the Galactic longitude. The error shows the 90 % confidence level.

4. Discussion

4.1. The 6.7 and 6.97 keV Lines

Thanks to the excellent energy resolution of the Suzaku XIS, the Fe line complex was clearly resolved into three narrow emission lines at ~ 6.4 , ~ 6.7 , and ~ 6.97 keV, and their spatial distribution along the Galactic plane was manifested. The 6.7 keV line is clearly found in all the Galactic Ridge and GC regions, indicating that a thin thermal hot plasma is located along the Galactic plane. The equivalent widths (EWs) of the 6.7 keV and 6.97 keV lines are ~ 300 – 980 eV and ~ 20 – 230 eV, respectively. The observed center energies of the 6.7 keV line are consistent with the theoretical value of Fe XXV in a collisional ionization equilibrium (CIE) plasma (6.68 keV), taking account of the statistical errors and the calibration uncertainty of the energy scale (0.2% at 6 keV, Koyama et al. 2007a). Furthermore, the flux ratios of the 6.97 keV/6.7 keV lines

are in good agreement with those expected from a CIE plasma with a temperature of 2–8 keV. Thus, our results support that the GRXE is likely to be thermal emission from a CIE plasma, as shown for the GCDX by Koyama et al. (2007c) and for one of the GRXE fields (R8) by Ebisawa et al. (2008).

4.2. The 6.4 keV Line

In addition to the 6.7 keV and 6.97 keV lines, the 6.4 keV emission line was found in various Galactic plane regions, which suggests omnipresence of the 6.4 keV line in the Galactic plane regions. The EW of the 6.4 keV line from the GRXE is < 400 eV. The GC region has been known to exhibit a strong 6.4 keV line, in particular strong enhancement of the 6.4 keV line flux at the Sgr B2 cloud was found with ASCA (Koyama et al. 1996). The Sgr B2 X-ray spectrum exhibited a strong 6.4 keV emission line with the EW of > 1 keV and an absorption edge of the neutral iron at 7.1 keV, which is well explained by reflection of X-rays from an external bright X-ray source (X-ray Reflection Nebula, XRN), where Sgr A* is presumably the irradiating source (Sunyaev et al. 1993; Koyama et al. 1996). Recently similar XRN objects have been found in the GC region with ASCA, Chandra, and Suzaku (Murakami et al. 2000, 2001a, 2001b; Park et al. 2004, Koyama et al. 2007b, 2008; Nobukawa et al. 2008). On the other hand, the GRXE fields are much far from the GC, thus the same XRN scenario as that in the GC region cannot be expected. Therefore, another scenario to produce the 6.4 keV emission line is required. Interactions between the interstellar medium and high-energy electrons or X-ray photons in the Galactic plane fields can produce the 6.4 keV lines. Assuming the diffuse origin of the GRXE, Valinia et al. (2000) proposed that interactions between the interstellar medium and cosmic-ray electrons are responsible for the 6.4 keV line. In this case, distribution of the 6.4 keV line intensity is expected to be spatially correlated with that of the molecular cloud, which may be observable in future.

If the GRXE is composition of numerous faint X-ray sources, the composite spectra must exhibit a similar spectrum to the GRXE, in particular the three narrow Fe emission lines at the energies of 6.4, 6.7, and 6.97 keV. Cataclysmic variables (CVs) and active binary stars (ABs) such as RS CVn type stars are proposed to be prime candidate populations of the GRXE (Revnivtsev et al. 2006). The X-ray spectrum of CVs exhibits a thermal emission with the 6.4, 6.7, and 6.97 keV lines (e.g., Hellier et al. 1998; Ezuka & Ishida 1999; Ishida et al. 2007; Mukai et al. 2007), while that of ABs exhibits a thermal emission with the 6.7 keV line but without the strong 6.4 keV line (e.g., Güdel et al. 1999). Consequently, the Fe line features of the GRXE, omnipresence of the 6.4 keV line in addition to the 6.7 keV and 6.97 keV lines, implies that CVs are major contributor to the flux of the GRXE, if the GRXE has the point source origin.

4.3. Fe Lines from CVs

Magnetic CVs (polars and intermediate polars), a subclass of CVs, are efficient X-ray emitters with luminosities of $\sim 10^{32}$ – 10^{33} erg s $^{-1}$, while the majority of CVs are non magnetic CVs, faint X-ray sources with luminosities of $\sim 10^{31}$ erg s $^{-1}$. At least 80% of non magnetic CVs are thought to be dwarf novae (e.g., Patterson 1984). According to Fe line properties of magnetic CVs summarized in Hellier et al. (1998) and Ezuka and Ishida (1999), the mean EWs of the 6.4 keV, 6.7 keV, and 6.97 keV lines are ~ 100 – 150 eV, ~ 200 eV, and ~ 100 eV, respectively. Suzaku results of dwarf novae, SS Cyg and V893 Sco (Ishida et al. 2007; Mukai et al. 2007) suggest that their Fe line features are similar to those of magnetic CVs. Comparing the Fe line features of the GRXE with those of CVs, we found that the 6.7 keV line EW of the GRXE (~ 300 – 980 eV) is larger than that of CVs, but the Fe line properties are similar to each other.

We estimate the space density of CVs which are required to explain all the observed Fe line flux of the GRXE. If the continuum emission of CVs is thin thermal emission from a hot plasma with a temperature of ~ 10 keV and the EW of the 6.4 keV line is 150 eV, the luminosity of the 6.4 keV line emission is estimated to be $\sim 1.5\%$ of the 2–10 keV luminosity. The longitudinal distribution of the GRXE shows a strong enhancement within the area of $|l| \leq 30^\circ$ (Yamauchi & Koyama 1993; Sugizaki et al. 2001; Revnivtsev et al. 2006), which corresponds to the Galactic inner disk with a radius of 4 kpc. For simplicity, we assumed that the CVs are uniformly distributed in the Galactic inner disk region with a radius (R_d) of 4 kpc and a height of 300 pc and the distance to the Galactic Center (R_0) is 8 kpc. Based on the results of X-ray observations of CVs (e.g., Cordova & Mason 1984; Mukai & Shiokawa 1993; Ezuka & Ishida 1999; Baskill et al. 2005; Sazonov et al. 2006), we also assumed the mean luminosity to be 10^{32} erg s $^{-1}$. Thus, the observed 6.4 keV line flux from the GRXE, $F_{6.4\text{keV}}$ (erg s $^{-1}$ cm $^{-2}$ str $^{-1}$), is expressed as follows.

$$F_{6.4\text{keV}} = \int \frac{n L_{6.4\text{keV}}}{4\pi} dx = \frac{n L_{6.4\text{keV}}}{4\pi} X, \quad (1)$$

where $L_{6.4\text{keV}}$, n , and X are a mean 6.4 keV line luminosity of CV ($= 1.5\%$ of 10^{32} erg s $^{-1}$), a space density of CV, and a length across the disk, respectively. In the case of the uniform disk model, X is $2\sqrt{R_d^2 - (R_0 \sin l)^2}$. Using the best-fit 6.4 keV line surface brightness, the required CV space density is calculated to be $\sim (0.6$ – $8.6) \times 10^{-5}$ pc $^{-3}$.

We also carried out the same estimation using the 6.7 keV line. If we assume the mean EW of the 6.7 keV line from CVs to be 200 eV, the 6.7 keV line luminosity is estimated to be $\sim 2\%$ of the 2–10 keV luminosity. Then, using the observed Fe line surface brightness from the GRXE, the required CV space density is calculated to be $(2.6$ – $21) \times 10^{-5}$ pc $^{-3}$.

The estimated CV space densities are larger than that of CVs observed in the Solar neighborhood so far ($\sim 6 \times 10^{-6}$ pc $^{-3}$, Patterson 1984). However, taking account of uncer-

tainties of the current estimation of the CV space density in the Galaxy, we cannot completely rule out the possibility that a large number of CVs are hiding inside the Galaxy. Or, if the mean luminosity of CVs turns out to be significantly larger than 10^{32} erg s $^{-1}$, the required CV space density can be much lower. For more precise estimation, construction of the luminosity function and a realistic model of the source distribution in the Galaxy are needed. Detailed measurements of the Fe line features of CVs are also useful. In any case, if the CV origin is correct, the reflection profile by the Compton scattering and the line broadening are expected, because the 6.4 keV emission line of CVs is emitted from the white dwarf surface and/or the accreting matter. A systematic energy shift of ~ 2 eV by the gravitational redshift is also expected. These features would be revealed by future X-ray micro-calorimeter missions.

4.4. The Flux Ratios of the Fe Lines

The 6.7 keV line is clearly found in all the GRXE and GCDX spectra, while the intensities of the ~ 6.4 keV and ~ 7 keV lines relative to that of the ~ 6.7 keV line seems to vary from field to field (figures 1 and 2). Figure 4 shows that there are some differences in the line flux ratios, although the errors are large. In particular, the line flux ratios of the GCDX are systematically larger than those of the GRXE. The 6.4 keV line would originate from a non thermal process. Here, we focus on the flux ratios of the other two lines in the thermal origin, the 6.97 keV/6.7 keV lines.

In order to examine the hypothesis that the line flux ratios observed at all the positions are the same, we fitted all the 6.97 keV/6.7 keV line flux ratios (GC1–4 and R1–8) with a constant model and obtained the reduced χ^2 value of 2.90 (the degree of freedom of 11). This means that the hypothesis is statistically rejected. Furthermore, the weighted mean values of the 6.97 keV/6.7 keV line flux ratio of the GCDX and the GRXE are 0.38 ± 0.02 and 0.22 ± 0.06 (90% confidence level), respectively. Thus, the line flux ratio of the GRXE is not the same as that of the GCDX. Based on the APEC model in XSPEC, the mean ratio for the GCDX (0.38) is corresponding to ~ 7 keV, while that for the GRXE (0.22) is ~ 5.5 keV. We also applied the same analysis to only the GRXE data (R1–8) and obtained the reduced χ^2 value of 0.49 (the degree of freedom of 7). From the statistical point of view, all the line flux ratio of the GRXE is considered to be the same. To examine the difference in the line ratios for the GRXE, we need good statistics data and more samples of the GRXE.

If the GRXE and the GCDX are composition of numerous faint X-ray sources, the spectra should be an averaged spectrum of the X-ray sources contributing to the GRXE and the GCDX. According to the results of the fluctuation analysis of the ASCA data (Sugizaki et al. 1999), more than 10^3 faint sources responsible for the GRXE should be included in the XIS FOV. In the case of the GCDX, the number of contributing sources should be larger because the 6.7 keV and 6.97 keV line fluxes of the GCDX

are more than 10 times larger than those of the GRXE. Hence, the GRXE and the GCDX spectra observed in the various regions are expected to be quite similar to each other. The difference in the 6.97 keV/6.7 keV line flux ratio suggests that at least the candidate sources in the GC region have a higher temperature plasma emission than those on the Galactic plane systematically.

On the other hand, if the GRXE has the diffuse origin, the difference in the line flux ratio of 6.97 keV/6.7 keV can be explained by spatial difference of the plasma temperature. If the hot plasma is produced by a process concerning the activity in the Galactic scale, the temperature distribution may be correlated with the Galactic structure. For example, the temperatures in the central parts are expected to be higher, while those in the outer regions and the off-plane regions are relatively low, which qualitatively agrees with the observation. More precise systematic study of the spatial distribution of the Fe lines is expected to give the answer in future.

5. Summary

We analyzed Suzaku data taken at various regions along the Galactic plane and studied their Fe-K emission line features. Suzaku resolved the Fe line complex into three narrow lines at ~ 6.4 keV, ~ 6.7 keV and ~ 6.97 keV, which are K-lines from neutral (or low-ionized), He-like, and H-like iron ions, respectively. The 6.7 keV line is clearly seen in all the observed regions and the 6.4 keV emission line was also found in various Galactic plane regions. The 6.4 keV/6.7 keV and the 6.97 keV/6.7 keV line flux ratios of the GCDX are found to be systematically larger than those of the GRXE.

Authors are grateful to all the members of the Suzaku team. This work was supported in part by the Grant-in-Aid for Scientific Research of the Japan Society for the Promotion of Science (JSPS) (No. 18540228, S.Y.).

References

- Balucinska-Church, M., & McCammon, D. 1992, *ApJ*, 400, 699
 Baskill, D. S., Wheatley, P. J., & Osborne, J. P. 2005, *MNRAS*, 357, 626
 Cordova, F. A., & Mason, K. O. 1984, *MNRAS*, 206, 879
 Ebisawa, K., Maeda, Y., Kaneda, H., & Yamauchi, S. 2001, *Science*, 293, 1633
 Ebisawa, K., et al. 2005, *ApJ*, 635, 214
 Ebisawa, K., et al. 2008, *PASJ*, 60, S223
 Ezuka, H., & Ishida, M. 1999, *ApJS*, 120, 277
 Gendreau, K. C., et al. 1995, *PASJ*, 47, L5
 Güdel, M., Linsky, J. L., Brown, A., & Nagase, F. 1999, *ApJ*, 511, 405
 Hellier, C., Mukai, K., & Osborne, J. P. 1998, *MNRAS*, 297, 526
 Ishida, M., Okada, S., Nakamura, R., Terada, Y., Hayashi, T., Mukai, K., & Hamaguchi, K. 2007, *Progress of Theoretical Physics Supplement*, 169, 178
 Kaneda, H., Makishima, K., Yamauchi, S., Koyama, K., Matsuzaki, K., & Yamasaki, N. Y. 1997, *ApJ*, 491, 638
 Kokubun, M., et al. 2007, *PASJ*, 59, S53
 Koyama, K., Makishima, K., Tanaka, Y., & Tsunemi, H. 1986, *PASJ*, 38, 121
 Koyama, K., Awaki, H., Kunieda, H., Takano, S., Tawara, Y., Yamauchi, S., Hatsukade, I., & Nagase, F. 1989, *Nature*, 339, 603
 Koyama, K., Maeda, Y., Sonobe, T., Takeshima, T., Tanaka, Y., & Yamauchi, S. 1996, *PASJ*, 48, 249
 Koyama, K., et al. 2007a, *PASJ*, 59, S23
 Koyama, K., et al. 2007b, *PASJ*, 59, S221
 Koyama, K., et al. 2007c, *PASJ*, 59, S245
 Koyama, K., Inui, T., Matsumoto, H., & Tsuru, T. G. 2008, *PASJ*, 60, S201
 Marshall, F. E., Boldt, E. A., Holt, S. S., Miller, R. B., Mushotsky, R. F., Rose, L. A., Rothschild, R. E., & Serlemitsos, P. J. 1989, *ApJ*, 235, 4
 Mitsuda, K., et al. 2007, *PASJ*, 59, S1
 Mukai, K., & Shiokawa, K. 1993, *ApJ*, 418, 863
 Mukai, K., Zietsman, E., & Still, M. 2007, *Progress of Theoretical Physics Supplement*, 169, 182
 Murakami, H., Koyama, K., Sakano, M., Tsujimoto, M., & Maeda, Y. 2000, *ApJ*, 534, 283
 Murakami, H., Koyama, K., & Maeda, Y. 2001a, *ApJ*, 558, 687
 Murakami, H., Koyama, K., Sakano, M., Tsujimoto, M., & Maeda, Y. 2001b, *ApJ*, 550, 297
 Nobukawa, M., et al. 2008, *PASJ*, 60, S191
 Park, S., Munro, M. P., Baganoff, F. K., Maeda, Y., Morris, M., Howard, C., Bautz, M. W., & Garmire, G. P. 2004, *ApJ*, 603, 548
 Patterson, J. 1984, *ApJS*, 54, 443
 Revnivtsev, M., & Sazonov, S. 2007, *A&A*, 471, 159
 Revnivtsev, M., Gilfanov, M., Jahoda, K., & Sunyaev, R. 2005, *A&A*, 444, 381
 Revnivtsev, M., Sazonov, S., Gilfanov, M., Churazov, E., & Sunyaev, R. 2006, *A&A*, 452, 169
 Sazonov, S., Revnivtsev, M., Gilfanov, M., Churazov, E., & Sunyaev, R. 2006, *A&A*, 450, 117
 Sakano, M., Koyama, K., Murakami, H., Maeda, Y., & Yamauchi, S. 2002, *ApJS*, 138, 19
 Serlemitsos, P., et al. 2007, *PASJ*, 59, S9
 Sugizaki, M., Matsuzaki, K., Kaneda, H., Yamauchi, S., Mitsuda, K., & the ASCA Galactic Plane Survey team 1999, *Astron. Nachr.*, 320, 383
 Sugizaki, M., Mitsuda, K., Kaneda, H., Matsuzaki, K., Yamauchi, S., & Koyama, K. 2001, *ApJS*, 134, 77
 Sunyaev, R. A., Markevitch, M., & Pavlinsky, M. 1993, *ApJ*, 497, 606
 Takahashi, T., et al. 2007, *PASJ*, 59, S35
 Tanaka, Y. 2002, *A&A*, 382, 1052
 Tawa, N., et al. 2008, *PASJ*, 60, S11
 Valinia, A., & Marshall, F. E. 1998, *ApJ*, 505, 134
 Valinia, A., Tatischeff, V., Arnaud, K., Ebisawa, K., & Ramaty, R. 2000, *ApJ*, 543, 733
 Warwick, R. S., Turner, M. J. L., Watson, M. G., Willingale, R. 1985, *Nature*, 317, 218
 Worrall, D. M., Marshall, F. E., Boldt, E. A., & Swank, J. H. 1982, *ApJ*, 255, 111
 Yamasaki, N. Y., et al. 1997, *ApJ*, 481, 821
 Yamauchi, S., Kawada, M., Koyama, K., Kunieda, H., Tawara, Y., Hatsukade, I. 1990, *ApJ*, 365, 532
 Yamauchi, S., & Koyama, K. 1993, *ApJ*, 404, 620

Yamauchi, S., Kaneda, H., Koyama, K., Makishima, K.,
Matsuzaki, K., Sonobe, T., Tanaka, Y., & Yamasaki, N.
1996, PASJ, 48, L15